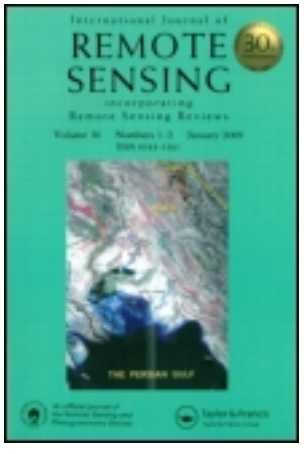

International Journal of Remote Sensing

Publication details, including instructions for authors and subscription information:
http://www.tandfonline.com/loi/tres20

Comparison of multisource image fusion methods and land cover classification

D. Amarsaikhan [a], M. Saandar [b], M. Ganzorig [a], H.H. Blotevogel [c], E. Egshiglen [a], R. Gantuyal [a], B. Nergui [a] & D. Enkhjargal [a]

[a] Institute of Informatics and RS, Mongolian Academy of Sciences, Ulaanbaatar-51, Mongolia

[b] Monmap Engineering Company, Ltd., Ulaanbaatar, 210646, Mongolia

[c] Faculty of Spatial Planning, Institute of Spatial Planning, Dortmund University of Technology, D-44221, Dortmund, Germany

Published online: 10 Oct 2011.

To cite this article: D. Amarsaikhan , M. Saandar , M. Ganzorig , H.H. Blotevogel , E. Egshiglen , R. Gantuyal , B. Nergui & D. Enkhjargal (2012): Comparison of multisource image fusion methods and land cover classification, International Journal of Remote Sensing, 33:8, 2532-2550

To link to this article: http://dx.doi.org/10.1080/01431161.2011.616552

International Journal of Remote Sensing
Vol. 33, No. 8, 20 April 2012, 2532–2550

Taylor & Francis
Taylor & Francis Group

Comparison of multisource image fusion methods and land cover classification

D. AMARSAIKHAN*†, M. SAANDAR‡, M. GANZORIG†,
H. H. BLOTEVOGEL§, E. EGSHIGLEN†, R. GANTUYAL†, B. NERGUI†
and D. ENKHJARGAL†

†Institute of Informatics and RS, Mongolian Academy of Sciences, Ulaanbaatar-51, Mongolia
‡Monmap Engineering Company, Ltd., Ulaanbaatar 210646, Mongolia
§Faculty of Spatial Planning, Institute of Spatial Planning, Dortmund University of Technology, D-44221 Dortmund, Germany

(*Received 24 June 2009; in final form 12 June 2011*)

The aim of this study is to explore the performances of different data fusion techniques for the enhancement of urban features and evaluate the features obtained by the fusion techniques in terms of separation of urban land cover classes when multisource images are under consideration. For the data fusion, multiplicative method, Brovey transform, principal component analysis (PCA), Gram–Schmidt fusion, wavelet-based fusion and Elhers fusion are used and the results are compared. Of these methods, the best result is obtained by the use of the optical/synthetic aperture radar (SAR) wavelet-based fusion. The classification methods of multisource images, statistical maximum likelihood classification (MLC) and the knowledge-based method are used and the results are compared. The knowledge-based method is based on a hierarchical rule-based approach and it uses a hierarchy of rules describing different conditions under which the actual classification has to be performed. Overall, the research indicates that multisource information can significantly improve the interpretation and classification of land-cover types and the knowledge-based method is a powerful tool in the production of a reliable land-cover map.

1. Introduction

Image fusion is used for many purposes. Very often, it is used to produce an image with an improved spatial resolution. The most common situation is represented by a pair of images where the first acquired by a multispectral sensor has a pixel size greater than the pixel size of the second image acquired by a panchromatic sensor. Combining these images, fusion produces a new multispectral image with a spatial resolution equal to the panchromatic one. In addition, image fusion introduces important distortion on the pixel spectra, which in turn improve the information content of remote-sensing (RS) images (Teggi *et al*. 2003). Over the years, different fusion methods have been developed for improving spatial and spectral resolutions of RS data sets. The techniques most encountered in the literature are the intensity-hue-saturation (IHS) transform, the Brovey transform, the principal component analysis (PCA) method, the Gram–Schmidt method, the local mean matching method, the local mean and

*Corresponding author. Email: amar64@arvis.ac.mn

International Journal of Remote Sensing
ISSN 0143-1161 print/ISSN 1366-5901 online © 2012 Taylor & Francis
http://www.tandf.co.uk/journals
http://dx.doi.org/10.1080/01431161.2011.616552

variance matching method, the least square fusion method, the wavelet-based fusion method, the multiplicative and the Ehlers fusion (Karathanassi *et al.* 2007, Ehlers *et al*. 2008). Most fusion applications use modified approaches or combinations of these methods.

In case of RS data sets, three different fusions, such as fusion of optical data with optical data, fusion of microwave data with microwave data and fusion of optical and microwave data sets, can be conducted. For several decades, fusion of multiresolution optical images has been successfully used for the improvement of information content of images for visual interpretation as well as for the enhancement of land surface features. Many studies have been conducted on the improvement of spatial resolution of multispectral images by the use of the high frequencies of panchromatic images, while preserving the spectral information (Mascarenha *et al.* 1996, Saraf 1999, Teoh *et al*. 2001, Teggi *et al*. 2003, Gonzalez *et al*. 2004, Colditz *et al.* 2006, Deng *et al.* 2008, Li and Leung 2009). A number of authors have attempted to successfully fuse the interferometric or multifrequency synthetic aperture radar (SAR) images (Soh and Tsatsoulis 1999, Verbyla 2001, Baghdadi *et al*. 2002, Costa 2005, Palubinskas and Datcu 2008). Unlike the fusion of optical images, most fusions of the SAR data sets have attempted to increase the spectral variety of the classes.

Over the years, the fusion of optical and SAR data sets has been widely used for different applications. It has been found that the images acquired at optical and microwave ranges of the electromagnetic spectrum provide unique information when they are integrated (Amarsaikhan *et al*. 2007). Now image fusion based on the integration of multispectral optical and multifrequency microwave data sets is being efficiently used for interpretation, enhancement and analysis of different land surface features. As is known, optical data contain information on the reflective and emissive characteristics of the Earth's surface features, while SAR data contain information on the surface roughness, texture and dielectric properties of natural and man-made objects. It is evident that a combined use of optical and SAR images will have a number of advantages because a specific feature which is not seen on the passive sensor image might be seen on the microwave image and vice versa because of the complementary information provided by the two sources (Amarsaikhan *et al*. 2004, 2007). Many authors have proposed and applied different techniques to combine optical and SAR images in order to enhance various features and they all judged that the results from the fused images were better than the results obtained from the individual images (Wang *et al*. 1995, Pohl and van Genderen 1998, Ricchetti 2001, Herold and Haack 2002, Amarsaikhan and Douglas 2004, Westra *et al*. 2005, Ehlers *et al*. 2008, Saadi and Watanabe 2009, Zhang 2010). Although many studies of image fusion have been conducted for derivation of new algorithms for the enhancement of different features, still little research has been done on the influence of image fusions on the automatic extraction of different thematic information within the urban environment.

For several decades, (single-source) multispectral RS data sets have been widely used for land cover mapping and, for the generation of land cover information, diverse classification methods have been applied (Storvik *et al*. 2005, Meher *et al*. 2007). Unlike single-source data, data sets from multiple sources have proved to offer better potential for discriminating between different land cover types. Many authors have assessed the potential of multisource images for the classification of different land cover classes (Munechika *et al*. 1993, Serpico and Roli 1995, Benediktsson *et al*. 1997, Hegarat-Mascle *et al*. 2000, Amarsaikhan and Douglas 2004, Amarsaikhan

et al. 2007). In RS applications, the most widely used multisource classification techniques are statistical methods, Dempster–Shafer theory of evidence, neural networks, and decision tree classifier and knowledge-based methods (Solberg *et al*. 1996, Franklin *et al.* 2002, Amarsaikhan *et al*. 2007).

Recently, mapping of urban areas, specifically at regional and global scales, has become an important task due to the increasing pressures from rapid urbanization and associated environmental problems (Cao *et al*. 2009). However, in most cases urban areas are complex and diverse in nature and many features have similar spectral characteristics and it is not easy to separate them by the use of ordinary feature combinations or by applying standard techniques. In order to successfully extract urban land cover classes, reliable features derived from multiple sources and an efficient classification technique should be used. The aim of this study is (a) to investigate different data fusion techniques for the enhancement of spectral variations of urban features and (b) to classify the features composed by the fusion techniques and produce a reliable urban land cover map. For data fusion, two different approaches such as fusion of SAR data with SAR data (i.e. SAR/SAR approach) and fusion of optical data with SAR data (i.e. optical/SAR approach) have been used. For the actual analysis, multisource data sets of an urban area in Mongolia have been used. The analysis was carried out using the personal computer (PC)-based Earth Resource Data Analysis System (ERDAS) Imagine 9.1 (ESRI, Redlands, CA, USA) and Environment for Visualizing Images (ENVI) 4.3. (ITT Visual Information Solutions, Boulder, CO, USA).

2. Test site and data sources

As a test site, Ulaanbaatar, the capital city of Mongolia, has been selected. Ulaanbaatar is situated in the central part of Mongolia, on the Tuul River, at an average height of 1350 m above sea level, and currently has about 1 million inhabitants. The city is surrounded by mountains, which are spurs of the Khentii Mountain Ranges. Founded in 1639 as a small town named Urga, today it has prospered as the main political, economic, business, scientific and cultural centre of the country.

The city extends from the west to the east about 30 km and from the north to the south about 20 km. However, the study area chosen for the present study covers mainly the central and western parts and is characterized by such classes as built-up area, ger (Mongolian national dwelling) area, green area, soil and water. Figure 1 shows an Advanced Spaceborne Thermal Emission and Reflection Radiometer (ASTER) image of the test site and some examples of its land cover.

In the present study, for the enhancement of urban features, ASTER data of 23 September 2008, European Remote-Sensing Satellite (ERS)-2 SAR data of 25 September 1997 and Advanced Land Observing Satellite (ALOS) Phased Array type L-band Synthetic Aperture Radar (PALSAR) data of 25 August 2006 have been used. Although ASTER has 14 multispectral bands acquired in visible, near infrared, middle infrared and thermal infrared ranges of electromagnetic spectrum, in the current study, green (band1), red (band2) and near infrared (band3) bands with a spatial resolution of 15 m have been used. ERS-2 SAR is a European RS radar satellite which acquires vertical (VV)-polarization C-band data with a spatial resolution of 25 m. ALOS PALSAR is a Japanese Earth-observation satellite carrying a cloud-piercing L-band radar, which is designed to acquire fully polarimetric images. In the present study, horizontal (HH), VV and cross (HV) polarization intensity images of ALOS

Figure 1. 2008 ASTER image of the selected part of Ulaanbaatar (Band 1 = blue, Band 2 = green, Band 3 = red). 1 – Built-up area; 2 – ger area; 3 – green area; 4 – soil; 5 – water. The size of the displayed area is about 8.01 km × 6.08 km.

PALSAR with spatial resolutions of 25 m have been used. VH polarization image was excluded, because it has the same intensity value as the HV polarization image.

3. Co-registration of multisource images and speckle suppression of the SAR images

At the beginning, the ALOS PALSAR image was rectified to the coordinates of the ASTER image using 12 ground control points (GCPs) defined from a topographic map of the study area. The GCPs have been selected on clearly delineated crossings of roads, streets and city building corners. For the transformation, a second-order transformation and nearest-neighbour resampling approach were applied and the related root mean square error (RMSE) was 0.94 pixels. Then, the ERS-2 SAR image was rectified and its coordinates were transformed to the coordinates of the rectified ALOS PALSAR image. In order to rectify the ERS-2 SAR image, 14 more regularly distributed GCPs were selected from different parts of the image. For the actual transformation, a second-order transformation was used. As a resampling technique, the nearest-neighbour resampling approach was applied and the related RMSE was 0.98 pixels.

As the microwave images have a granular appearance due to the speckle formed as a result of the coherent radiation used for radar systems, the reduction of the speckle is a very important step in further analysis. Analysis of the radar images must be based on techniques that remove the speckle effects while considering the intrinsic texture of the image frame (Amarsaikhan and Douglas 2004, Serkan *et al*. 2008). In this study, four different speckle suppression techniques such as local region, Lee sigma, Frost and gamma map filters (ERDAS 1999) of 3 × 3 and 5 × 5 sizes were compared in terms of delineation of urban features and texture information. After visual inspection of each image, it was found that the 3 × 3 gamma map filter created the best images in terms of delineation of different features as well as preserving the content of texture information. In the output images, speckle noise was reduced with very low degradation of the textural information.

4. Image fusion

The concept of image fusion refers to a process which integrates different images from different sources to obtain more information, considering a minimum loss or distortion of the original data. In other words, the image fusion is the integration of different digital images in order to create a new image and obtain more information than can be separately derived from any of them (Pohl and van Genderen 1998, Ricchetti 2001, Amarsaikhan *et al*. 2009). In the case of the present study, for the urban areas, the radar images provide structural information about buildings and street alignment due to the double bounce effect, while the optical image provides information about the spectral variations of different urban features. Moreover, the SAR images contain multitemporal changes of land surface features and provide some additional information about soil moisture conditions due to the dielectric properties of the soil. Over the years, different data fusion techniques have been developed and applied, individually and in combination, providing users and decision-makers with various levels of information. Generally, image fusion can be performed at pixel, feature and decision levels (Abidi and Gonzalez 1992, Pohl and van Genderen 1998). In this study, data fusion has been performed at a pixel level and the following rather common and more complex techniques were compared: (a) the multiplicative method, (b) the Brovey transform, (c) PCA, (d) Gram–Schmidt fusion (e) wavelet-based fusion and (f) Elhers fusion. Each of these techniques is briefly discussed below.

Multiplicative method. This is the most simple image fusion technique. It takes two digital images, for example, high-resolution panchromatic and low-resolution multispectral data, and multiplies them pixel by pixel to get a new image (Seetha *et al*. 2007).

Brovey transform. This is a simple numerical method used to merge different digital data sets. The algorithm based on a Brovey transform uses a formula that normalizes multispectral bands used for a red, green, blue colour display and multiplies the result by high-resolution data to add the intensity or brightness component of the image (Vrabel 1996).

PCA. The most common understanding of the PCA is that it is a data compression technique used to reduce the dimensionality of the multidimensional data sets (Richards and Jia 1999). It is also helpful for image encoding, enhancement, change detection and multitemporal dimensionality (Pohl and van Genderen 1998). PCA is a statistical technique that transforms a multivariate data set of intercorrelated variables into a set of new uncorrelated linear combinations of the original variables, thus generating a new set of orthogonal axes.

Gram–Schmidt fusion method. The Gram–Schmidt process is a procedure which takes a non-orthogonal set of linearly independent functions and constructs an orthogonal basis over an arbitrary interval with respect to an arbitrary weighting function. In other words, this method creates from the correlated components non- or less-correlated components by applying an orthogonalization process. Generally, orthogonalization is important in diverse applications in mathematics and other applied sciences because it can often simplify calculations or computations by making it possible, for example to do the calculation in a recursive manner (Karathanassi *et al.* 2007).

Wavelet-based fusion. The wavelet transform decomposes the signal based on elementary functions, that is, the wavelets. By using this, an image is decomposed into a set of multiresolution images with wavelet coefficients. For each level, the coefficients contain spatial differences between two successive resolution levels. In general, a wavelet-based image fusion can be performed either by replacing some wavelet

coefficients of the low-resolution image by the corresponding coefficients of the high-resolution image or by adding high-resolution coefficients to the low-resolution data (Pajares and Cruz 2004). In this study, the first approach, which is based on bi-orthogonal transforms, has been applied.

Elhers fusion. This is a fusion technique used for the spectral characteristic preservation of multitemporal and multisensor data sets. The fusion is based on an IHS transformation combined with filtering in the Fourier domain and the IHS transform is used for optimal colour separation. As the spectral characteristics of the multispectral bands are preserved during the fusion process, there is no dependency on the selection or order of bands for the IHS transform (Ehlers 2004, Ehlers *et al*. 2008).

4.1 *Comparison of the fusion methods using the SAR/SAR approach*

Generally, interpretation of microwave data is based on the backscatter properties of the surface features, and most SAR image analyses are based on them. Below, the backscatter characteristics of the available five classes have been described. In the case of two urban classes (i.e. built-up and ger areas), at both L-band and C-band frequencies the backscatter would contain information about street alignment, a building's size, density, roofing material and orientation, vegetation and soil, that is, it would contain all kinds of scattering. Roads and buildings can reflect a larger component of radiation if they are aligned at right angles to the incident radiation. Here, the intersection of a road and a building tends to act as a corner reflector. The amount of backscatter is very sensitive to street alignment. The areas of streets and buildings aligned at right angles to the incident radiation will have very a bright appearance and non-aligned areas will have a darker appearance in the resulting image. Volume and surface scattering will also play an important role in the response from urban areas. Therefore, these classes will have a higher backscatter return resulting in bright appearances on the images.

In the study site, the green area consists of some forest and vegetated surface. In the case of forest, at the L-band frequency the wavelength will penetrate to the forest canopy and will cause volume scattering to be derived from multiple-path reflections among twigs, branches, trunks and the ground, while at the C-band frequency only volume scattering from the top layer can be expected, because the wavelength is too short to penetrate to the forest layer. The vegetated surface will act as mixtures of small bush, grass and soil and the backscatter will depend on the volume of either of them. Also plant geometry, density and water content are the main factors influencing the backscatter coming from the vegetation cover. As a result, green areas will have a brighter appearance on the image. The backscatter of soil depends on the surface roughness, texture, existing surface patterns, moisture content, as well as the wavelength and incident angle. The presence of water strongly affects the microwave emissivity and reflectivity of a soil layer. At low moisture levels, there is a low increase in the dielectric constant. Above a critical amount, the dielectric constant rises rapidly. This increase occurs when moisture begins to operate in a free space and the capacity of a soil to hold and retain moisture is directly related to the texture and structure of the soil. As can be seen, soil will have a brighter appearance if it is wet and a dark appearance if it is dry. Water should have the lowest backscatter values and a dark appearance at both frequencies because of its specular reflection, which causes less reflection towards the radar antenna.

As can be seen from figure 2, the images created by the multiplicative method, Brovey transform and Gram–Schmidt fusion have very similar appearances. On

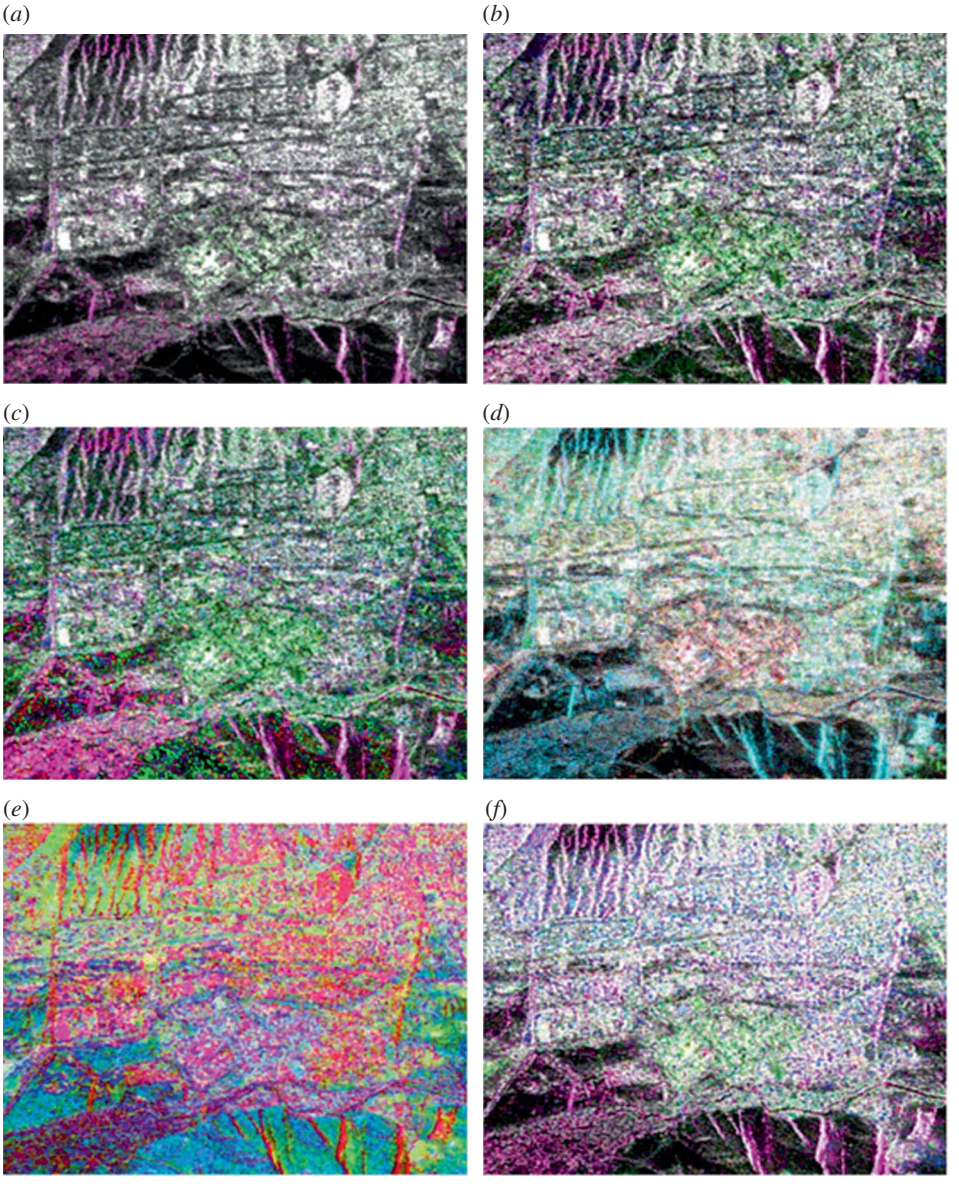

Figure 2. Comparison of the fused images of ALOS PALSAR and ERS-2 SAR of the selected part of Ulaanbaatar: (*a*) the image obtained by the multiplicative method; (*b*) the Brovey transformed image; (*c*) the PC image (red – PC1, green – PC2, blue – PC3); (*d*) the image obtained by Gram–Schmidt fusion; (*e*) the image obtained by wavelet-based fusion; and (*f*) the image obtained by Elhers fusion.

these images, the built-up and ger areas have either similar (figure 2(*b*)) or mixed appearances (figure 2(*a*) and (*d*)). The green area has a similar appearance to the built-up area. This means that the backscatter from the double bounce effect in the built-up area has a similar power to the volume and diffuse scattering from the green area. Moreover, it is seen that on all images (except the principal component (PC) image), soil and water classes have dark appearances because of their specular

reflection (although in some areas wet soil has increased brightness). As the original bands have been transformed to the new principal components, it is not easy to recognize the available classes on the image created by the PCA (figure 2(*c*)). On the PC image, the two urban classes, some roads aligned at right angles to the radar antenna and some areas affected by radar layover, have magenta-reddish appearances, while other classes form different mixed classes. On the image created by the wavelet-based fusion (figure 2(*e*)), it is not possible to distinguish much detail. On this image, the two urban classes and green area as well as soil and water classes have similar appearances. Furthermore, it is seen that the image created by the Elhers fusion (figure 2(*f*)) looks similar to the image created by the Gram–Schmidt fusion, but has more light appearances. Overall, it is seen that the fused SAR images cannot properly distinguish the available spectral classes.

4.2 *Comparison of the fusion methods using optical/SAR approach*

Initially, the aforementioned fusion methods have been applied to such combinations as ASTER and HH, HV and VV polarization components of PALSAR as well as ASTER and ERS-2 SAR. Then, to obtain good colour images that can illustrate spectral and spatial variations of the classes of objects on the images, the fused images have been visually compared. In the case of the multiplicative method, the fused image of ASTER and PALSAR HH polarization (figure 3(*a*)) demonstrated a better result compared to other combinations, while in the case of the Brovey transform the combination of ASTER and ERS-2 SAR (figure 3(*b*)) created a good image. On the image obtained by the multiplicative method, the built-up and ger areas have similar appearances; however, the green area, soil and water classes have total separations. Likewise, on the image obtained by the Brovey transform, the built-up and ger areas have similar appearances, whereas the green area and soil classes have total separations. Moreover, on this image, a part of the water class is mixed with other classes.

PCA has been applied to such combinations as ASTER and ERS-2 SAR, ASTER and PALSAR and ASTER, PALSAR and ERS-2 SAR. When the results of the PCA were compared, the combination of ASTER, PALSAR and ERS-2 SAR demonstrated the best result compared to the other two combinations. The result of the final PCA is shown in table 1. As can be seen from table 1, PALSAR HH polarization and ERS-2 SAR have very high negative loadings in PC1 and PC2. In these PCs, visible bands of ASTER also have moderate to high loadings. This means that PC1 and PC2 contain the characteristics of both optical and SAR images. Although PC3 contained 7.0% of the overall variance and had moderate to high loadings of ASTER band1, PALSAR HH polarization and ERS-2 SAR, visual inspection revealed that it contained less information related to the selected classes. However, visual inspection of PC4, which contained 5.6% of the overall variance, in which VV polarization of PALSAR has a high loading, revealed that this feature contained useful information related to the textural difference between the built-up and ger areas. Inspection of the last PCs indicated that they contained noise from the total data set. The image obtained by the PCA is shown in figure 3(*c*). As can be seen from figure 3(*c*), although the PC image could separate the two urban classes, in some parts of the image, it created a mixed class of green area and soil.

In the case of the Gram–Schmidt fusion, the integrated image of ASTER and ERS-2 SAR (figure 3(*d*)) demonstrated a better result compared to other combinations. The image contained some layover effects available on the ERS-2 image and

looked very similar to the image obtained by the multiplicative method. In the case of the wavelet-based fusion, the fused image of ASTER and ERS-2 SAR (figure 3(*e*)) demonstrated a better result compared to other combinations, too. Also, this image looked better than any other images obtained by other fusion methods. On this image, all available five classes could be distinguished by their spectral properties. Moreover,

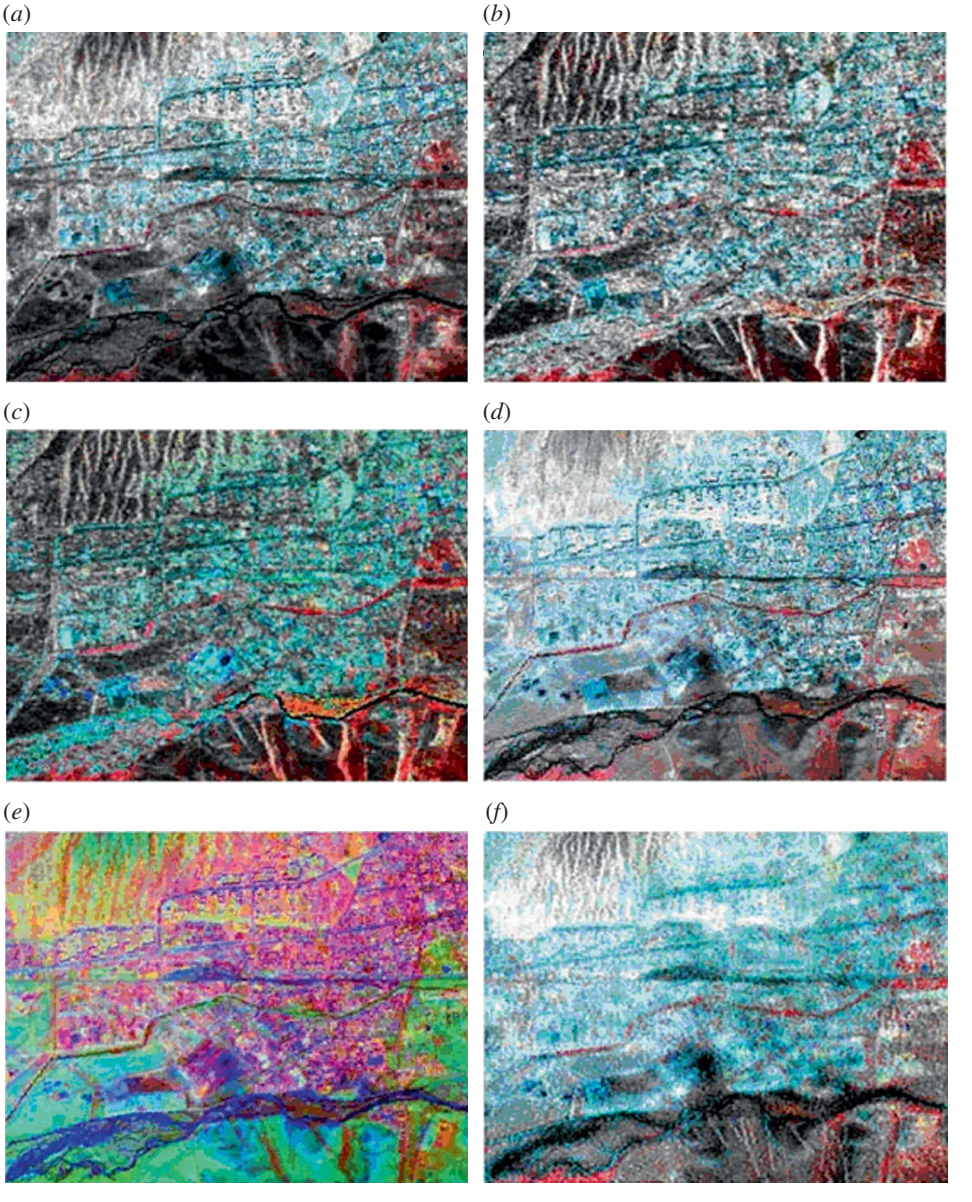

Figure 3. Comparison of the fused optical and SAR images: (*a*) the image obtained by the multiplicative method (ASTER and PALSAR HH); (*b*) the Brovey transformed image (ASTER and ERS-2 SAR); (*c*) the PC image (red – PC1, green – PC2, blue – PC3); (*d*) the image obtained by Gram–Schmidt fusion (ASTER and ERS-2 SAR); (*e*) the image obtained by wavelet-based fusion (ASTER and ERS-2 SAR); and (*f*) the image obtained by Elhers fusion (ASTER and PALSAR VV).

Table 1. Principal component coefficients from ASTER, PALSAR and ERS-2 SAR images.

	PC1	PC2	PC3	PC4	PC5	PC6	PC7
ASTER band1	0.33	0.44	0.42	0.35	0.44	0.39	0.17
ASTER band2	0.50	0.37	0.34	−0.34	−0.38	−0.33	−0.32
ASTER band3	0.02	0.07	0.11	−0.09	−0.32	−0.19	0.91
PALSAR HH	−0.77	0.34	0.47	−0.14	0.06	−0.15	−0.08
PALSAR HV	0.14	−0.07	−0.06	−0.49	0.73	−0.40	0.13
PALSAR VV	0.02	−0.01	0.01	0.69	0.08	−0.71	−0.04
ERS-2 SAR	0.07	−0.73	0.67	0.01	−0.01	0.02	−0.01
Eigenvalues	8873.3	4896.7	1159.7	934.6	459.2	147.7	81.7
Variance (%)	53.6	29.6	7.0	5.6	2.8	0.89	0.51

it could be seen that some textural information has been added for differentiation between the classes: built-up area and ger area. In the case of the Elhers fusion, the integrated image of ASTER and PALSAR VV polarization (figure 3(*f*)) demonstrated a better result compared to other combinations. Although this image had a blurred appearance due to speckle noise, it still could very well separate green area, soil and water classes. Figure 3 shows the comparison of the images obtained by different fusion methods.

5. Evaluation of features and urban land cover classification

5.1 *Evaluation of features using supervised classification*

Initially, in order to define the sites for the training signature selection, from the multisensor images, two to four areas of interest (AOI) representing the selected five classes (built-up area, ger area, green area, soil and water) have been selected through thorough analysis using a polygon-based approach. The separability of the training signatures was first checked in feature space and then evaluated using the transformed-divergence (TD) separability measure (table 2). The values of the TD separability measure range from 0 to 2000 and indicate how well the selected pairs are statistically separate. Values greater than 1900 indicate that the pairs have good separability (ENVI 1999, ERDAS 1999). After the investigation, the samples that demonstrated the greatest separability were chosen to form the final signatures. The final signatures included 2669 pixels for built-up area, 592 pixels for ger area, 241 pixels for green area, 1984 pixels for soil and 123 pixels for water.

In general, urban areas are complex and diverse in nature and many features have similar spectral characteristics, and it is not easy to separate them by the use of ordinary feature combinations. For the successful extraction of the urban land cover classes, reliable features derived from different sources should be used. In many cases, texture features derived from the occurrence and co-occurrence measures are used as

Table 2. The separabilities measured by the TD separability measure.

	Built-up area	Ger area	Green area	Soil	Water
Built-up area	0	787	1987	844	2000
Ger area	787	0	1999	1706	2000
Green area	1987	1999	0	1903	2000
Soil	844	1706	1903	0	2000
Water	2000	2000	2000	2000	0

additional reliable sources (Amarsaikhan *et al*. 2010). However, in the present study, the main objective was to evaluate the features obtained by the use of different fusion approaches. Therefore, for the classification, the following feature combinations were used:

1. the features obtained by the use of the multiplicative method using a SAR/SAR approach;
2. the features obtained by the use of the multiplicative method using a optical/SAR approach;
3. the features obtained by the use of the Brovey transform using a SAR/SAR approach;
4. the features obtained by the use of the Brovey transform using an optical/SAR approach;
5. the PC1, PC2 and PC3 of the PCA obtained using a SAR/SAR approach;
6. the PC1, PC2 and PC4 of the PCA obtained using an optical/SAR approach;
7. the features obtained by the use of the Gram–Schmidt fusion using a SAR/SAR approach;
8. the features obtained by the use of the Gram–Schmidt fusion using an optical/SAR approach;
9. the features obtained by the use of the wavelet-based fusion using a SAR/SAR approach;
10. the features obtained by the use of the wavelet-based fusion using an optical/SAR approach;
11. the features obtained by the use of the Elhers fusion using a SAR/SAR approach;
12. the features obtained by the use of the Elhers fusion using an optical/SAR approach;
13. the combined features of ASTER and PALSAR;
14. the combined features of ASTER and ERS-2 SAR; and
15. the combined features of ASTER, PALSAR and ERS-2 SAR.

For the actual classification, a supervised statistical maximum likelihood classification (MLC) has been used assuming that the training samples have the Gaussian distribution (Richards and Jia 1999). The final classified images are shown in figure 4(*a*)–(*o*). As seen from figure 4(*a*)–(*o*), the classification results of the SAR/SAR approach give the worst results, because there are high overlaps among classes: built-up area, ger area, soil and green area. However, these overlaps decrease in other images for the classification of which SAR as well as optical bands have been used. As could be seen from the overall classification results (table 3), although the combined use of optical and microwave data sets produced a better result than the single-source image, it is still very difficult to obtain a reliable land cover map by the use of the standard technique, specifically on decision boundaries of the statistically overlapping classes.

For the accuracy assessment of the classification results, the overall performance has been used. This approach creates a confusion matrix in which reference pixels are compared with the classified pixels and as a result an accuracy report is generated indicating the percentages of the overall accuracy (Mather 1999). As ground truth information, different AOIs containing 12 578 purest pixels have been selected. AOIs were selected on the principle that more pixels should be selected for the evaluation of the larger classes such as built-up area and ger area than the smaller classes such as green area and water. The overall classification accuracies for the selected classes are shown in table 3.

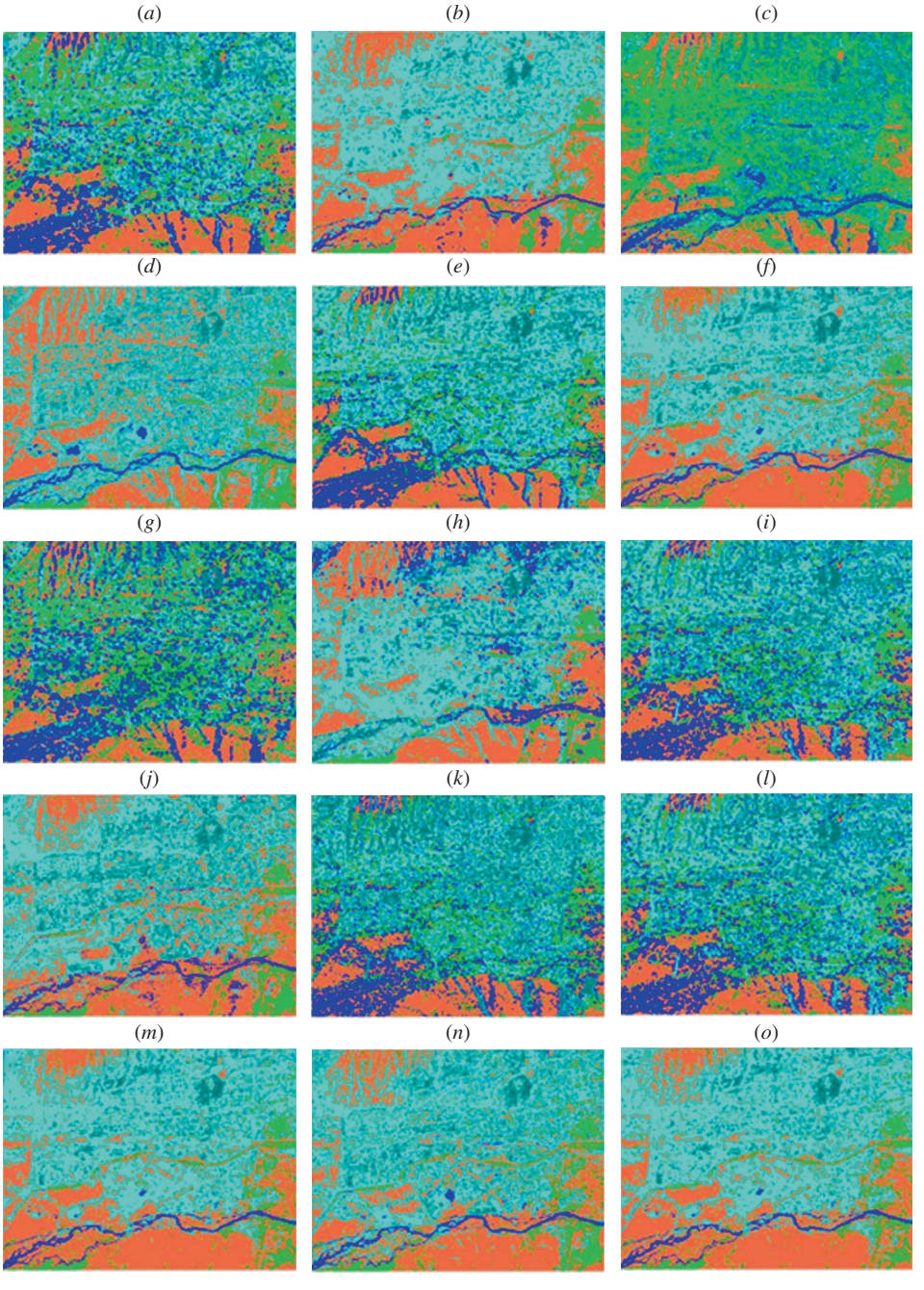

Figure 4. Comparison of the MLC results for the selected classes (cyan – built-up area; dark cyan – ger area; green – green area; sienna – soil; blue – water). Classified images of (*a*) the multiplicative method using a SAR/SAR approach, (*b*) the multiplicative method using an optical/SAR approach, (*c*) the Brovey transform using a SAR/SAR approach, (*d*) the Brovey transform using an optical/SAR approach, (*e*) PCA using a SAR/SAR approach, (*f*) PCA using an optical/SAR approach, (*g*) Gram–Schmidt fusion using a SAR/SAR approach, (*h*) Gram–Schmidt fusion using an optical/SAR approach, (*i*) wavelet-based fusion using a SAR/SAR approach, (*j*) wavelet-based fusion using an optical/SAR approach, (*k*) Elhers fusion using a SAR/SAR approach, (*l*) Elhers fusion using an optical/SAR approach, (*m*) features of ASTER and PALSAR, (*n*) features of ASTER and ERS-2 SAR and (*o*) features of ASTER, PALSAR and ERS-2 SAR.

Table 3. The overall classification accuracy of the classified images.

The bands (features) used for the MLC	Overall accuracy (%)
Multiplicative method using a SAR/SAR approach	46.12
Multiplicative method using an optical/SAR approach	78.17
Brovey transform using a SAR/SAR approach	41.57
Brovey transform using an optical/SAR approach	74.34
PCA using a SAR/SAR approach	71.83
PCA using an optical/SAR approach	81.92
Gram–Schmidt fusion using a SAR/SAR approach	40.86
Gram–Schmidt fusion using an optical/SAR approach	74.08
Wavelet-based fusion using a SAR/SAR approach	65.78
Wavelet-based fusion using an optical/SAR approach	76.26
Elhers fusion using a SAR/SAR approach	51.72
Elhers fusion using an optical/SAR approach	60.08
ASTER and PALSAR	79.98
ASTER and ERS-2 SAR	78.43
ASTER, PALSAR and ERS-2 SAR	80.12

5.2 *Knowledge-based classification*

In years past, knowledge-based techniques have been widely used for the classification of different RS images. The knowledge in image classification can be represented in different forms depending on the type of knowledge and necessity of its usage. The most commonly used techniques for knowledge representation are a rule-based approach and neural network classification (Amarsaikhan and Douglas 2004). In the present study, for separation of the statistically overlapping classes, a rule-based algorithm has been constructed. A rule-based approach uses a hierarchy of rules or a decision tree describing the conditions under which a set of low-level primary objects becomes abstracted into a set of high-level object classes. The primary objects contain the user-defined variables and include geographical objects represented in different structures, external programmes, scalars and spatial models (ERDAS 1999).

The constructed rule-based algorithm consists of two main hierarchies. In the upper hierarchy, on the basis of knowledge about reflecting and backscattering characteristics of the selected five classes, a set of rules which contain the initial image classification procedure based on a Mahalanobis distance rule and the constraints on spatial thresholds were constructed. It is clear that a spectral classifier will be ineffective if applied to the statistically overlapping classes such as built-up area and ger area because they have very similar spectral characteristics in both optical and microwave ranges. For such spectrally mixed classes, classification accuracies can be improved if the spatial properties of the classes of objects could be incorporated into the classification criteria. The spatial thresholds can be determined on the basis of historical thematic spatial data sets or from local knowledge about the site. In this study, the spatial thresholds were defined based on local knowledge about the test area.

In the initial image classification, for separation of the statistically overlapping classes, only pixels falling outside of the spatial thresholds and the PC1, PC2 and PC4 of the PCA obtained using optical/SAR approach were used. The pixels falling outside of the spatial thresholds were temporarily identified as unknown classes and further classified using the rules in which other spatial thresholds were used. As can be seen from the pre-classification analysis, there are different statistical overlaps among the classes, but significant overlaps exist among the classes: built-up area, ger area and soil. In the lower hierarchy of the rule base, different rules for the separation of

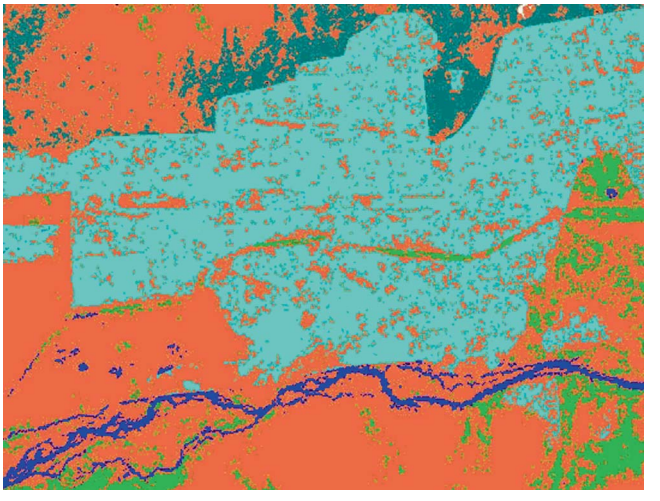

Figure 5. Classification result obtained by the knowledge-based classification (cyan – built-up area; dark cyan – ger area; green – green area; sienna – soil; blue – water).

these overlapping classes were constructed using spatial thresholds. The image classified by the constructed method is shown in figure 5. For the accuracy assessment of the classification result, the overall performance has been used, taking the same number of sample points as in the previous classifications. The confusion matrix produced for the knowledge-based classification showed overall accuracy of 90.92%. In order to allow an evaluation of the class-by-class results, confusion matrices of the

Table 4. Comparison of the detailed overall accuracies as well as users' and producers' accuracies of the classified images using the (a) knowledge-based classification and (b) supervised classification (ASTER, PALSAR and ERS-2 SAR).

	Reference data					
Classified data	Built-up area	Ger area	Green area	Soil	Water	Users' accuracy (%)
(a)						
Built-up area	5212	0	0	267	0	95.1
Ger area	187	1305	0	77	0	83.2
Green area	18	0	911	61	0	92.0
Soil	297	98	126	3771	0	87.9
Water	0	0	0	11	237	95.6
Total	5714	1403	1037	4187	237	
Producers' accuracy (%)	91.2	93.0	87.8	90.0	100.0	
(b)						
Built-up area	4902	407	18	980	28	77.4
Ger area	567	980	19	52	0	60.6
Green area	98	16	868	0	0	88.4
Soil	109	0	132	3136	17	92.4
Water	38	0	0	19	192	77.1
Total	5714	1403	1037	4187	237	
Producers' accuracy (%)	85.8	69.9	83.7	74.9	81.0	

Note: Overall accuracy for (a) is 90.92% (11 436/12 578) and (b) is 80.12% (10 078/12 578).

overall classification accuracies as well as users' and producers' accuracies of the classified images using the knowledge-based classification and the best supervised classification (ASTER, PALSAR and ERS-2 SAR) are given in table 4. As could be seen

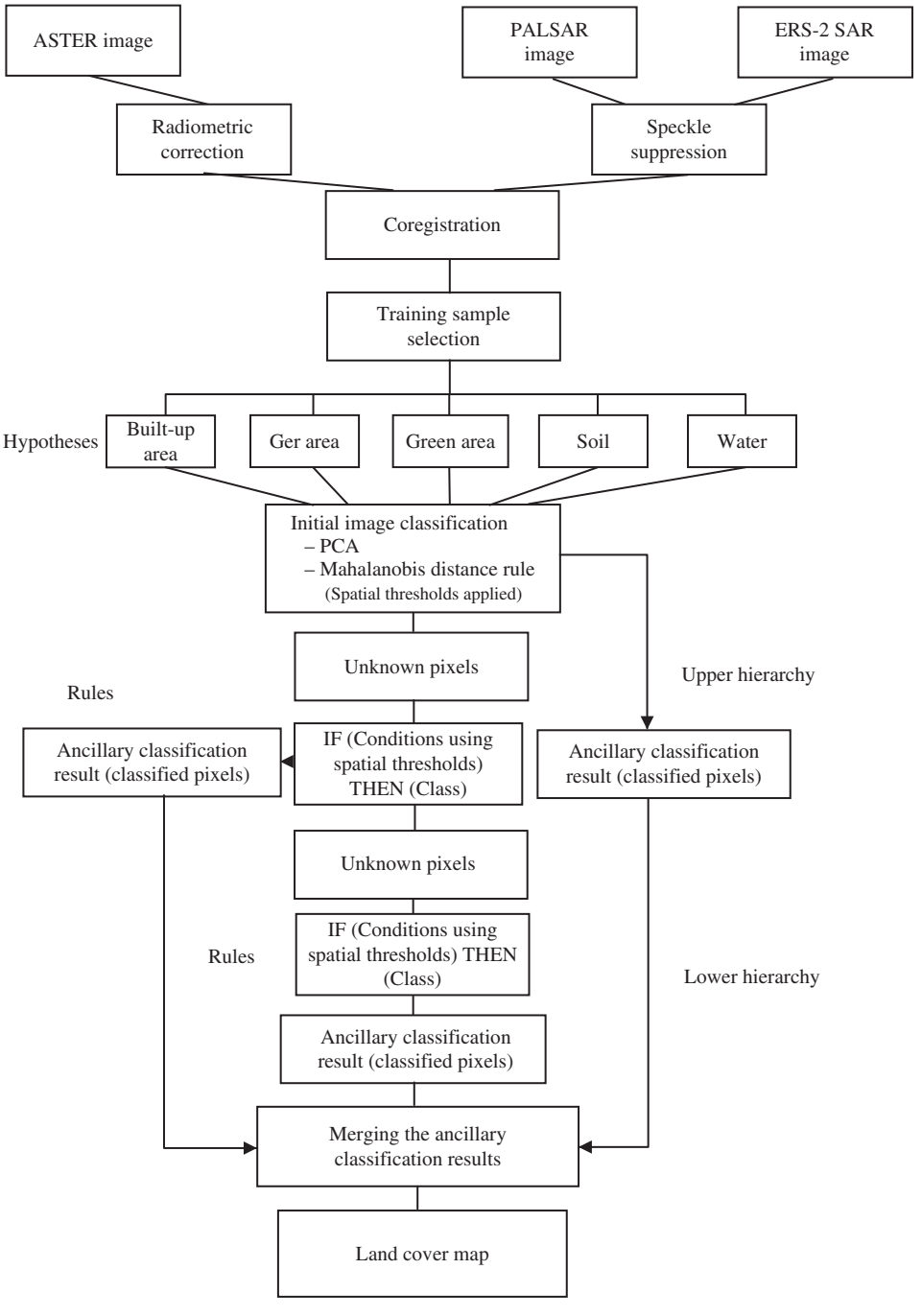

Figure 6. Flowchart of the constructed knowledge-based classification.

from figure 5 and table 4, the result of the classification using the rule-based method is much better than the result of the standard method. The flowchart of the constructed rule-based classification procedure is shown in figure 6.

6. Conclusions

The main aim of the research was to compare the performances of different data fusion techniques for the enhancement of different surface features and evaluate the features obtained by the fusion techniques in terms of separation of urban land cover classes. For the data fusion, two different approaches such as fusion of SAR data with SAR data and fusion of optical data with SAR data were considered. The fusion techniques, multiplicative method, Brovey transform, PCA, Gram–Schmidt fusion, wavelet-based fusion and Elhers fusion, were applied. In the case of the SAR/SAR approach, the fused SAR images could not properly distinguish the available spectral classes. In the case of the optical/SAR approach, although fusion methods demonstrated different results, detailed analysis of each image revealed that the image obtained by the wavelet-based fusion gave a superior image in terms of the spatial and spectral separations among different urban features. For the classification of the fused images, statistical MLC and the knowledge-based method were used and the results were compared. As could be seen from the classification results, the performance of the knowledge-based technique was much better than the performance of the standard method. Overall, the research indicated that multisource information can significantly improve the interpretation and classification of land cover classes and the knowledge-based method is a powerful tool in the production of a reliable land cover map.

Acknowledgement

A part of this research was conducted under the sponsorship for Humboldt Fellows.

References

Abidi, M.A. and Gonzalez, R.C., 1992, *Data Fusion in Robotics and Machine Intelligence* (New York: Academic Press).

Amarsaikhan, D., Blotevogel, H.H., Ganzorig, M. and Moon, T.H., 2009, Applications of remote sensing and geographic information systems for urban land-cover changes studies. *Geocarto International: A Multi-disciplinary Journal of Remote Sensing and GIS*, **24**, pp. 257–271.

Amarsaikhan, D., Blotevogel, H.H., van Genderen, J.L., Ganzorig, M., Gantuya, R. and Nergui, B., 2010, Fusing high resolution TerraSAR and Quickbird images for urban land cover study in Mongolia. *International Journal of Image and Data Fusion*, **1**, pp. 83–97.

Amarsaikhan, D. and Douglas, T., 2004, Data fusion and multisource data classification. *International Journal of Remote Sensing*, **17**, pp. 3529–3539.

Amarsaikhan, D., Ganzorig, M., Ache, P. and Blotevogel, H.H., 2007, The integrated use of optical and InSAR data for urban land cover mapping. *International Journal of Remote Sensing*, **28**, pp. 1161–1171.

Amarsaikhan, D., Ganzorig, M., Batbayar, G., Narangerel, D. and Tumentsetseg, S.H., 2004, An integrated approach of optical and SAR images for forest change study. *Asian Journal of Geoinformatics*, **3**, pp. 27–33.

Baghdadi, N., King, N., Bourguignon, A. and Remond, A., 2002, Potential of ERS and Radarsat data for surface roughness monitoring over bare agricultural fields: application to catchments in Northern France. *International Journal of Remote Sensing*, **23**, pp. 3427–3442.

Benediktsson, J.A., Sveinsson, J.R., Atkinson, P.M. and Tatnali, A., 1997, Feature extraction for multisource data classification with artificial neural networks. *International Journal of Remote Sensing*, **18**, 727–740.

Cao, X., Chen, J., Imura, H. and Higashi, O., 2009, A SVM-based method to extract urban areas from DMSP-OLS and SPOT VGT data. *Remote Sensing of Environment*, **10**, pp. 2205–2209.

Colditz, R.R., Wehrmann, T., Bachmann, M., Steinnocher, K., Schmidt, M., Strunz, G. and Dech, S., 2006, Influence of image fusion approaches on classification accuracy: a case study. *International Journal of Remote Sensing*, pp. 3311–3335. Available online at: http://www.informaworld.com/smpp/title~content=t713722504~db=all~tab=issueslist~branches=27 - v2727

Costa, M., 2005, Estimate of net primary productivity of aquatic vegetation of the Amazon floodplain using Radarsat and JERS-1. *International Journal of Remote Sensing*, **26**, pp. 4527–4536.

Deng, J.S., Wang, K., Deng, K.D. and Qi, G.J., 2008, PCA-based land-use change detection and analysis using multitemporal and multisensor satellite data. *International Journal of Remote Sensing*, pp. 4823–4838. Available online at: http://www.informaworld.com/smpp/title~content=t713722504~db=all~tab=issueslist~branches=29 - v2929

Ehlers, M., 2004. Spectral characteristics preserving image fusion based on Fourier domain filtering. In *Remote Sensing for Environmental Monitoring, GIS Applications, and Geology IV, Proceedings of Society of Photographic Instrumentation Engineers*, Bellingham, WA, pp. 93–116.

Ehlers, M., Klonus, S. and Åstrand, P.J., 2008, Quality assessment for multi-sensor multidate image fusion. In *CD-ROM Proceedings of the ISPRS Congresses*, 3–11 July 2008, Beijing, China.

ENVI, 1999, *User's Guide* (Boulder, CO: ITT Visual Information Solutions).

ERDAS, 1999, *Field Guide*, 5th ed. (Atlanta, GA: ERDAS).

Franklin., S.E., Peddle, D.R., Dechka, J.A. and Stenhouse, G.B., 2002, Evidential reasoning with Landsat TM, DEM and GIS data for landcover classification in support of grizzly bear habitat mapping. *International Journal of Remote Sensing*, pp. 4633–4652. Available online at: http://www.informaworld.com/smpp/title~content=t713722504~db=all~tab=issueslist~branches=23 - v2323

Gonzalez, A.M., Saleta, J.L., Catalan, R.G. and Garcia, R., 2004, Fusion of multispectral and panchromatic images using improved IHS and PCA mergers based on wavelet decomposition. *IEEE Transactions Geoscience and Remote Sensing*, **6**, pp. 1291–1299.

Hegarat-Mascle, S.L., Quesney, A., Vidal-Madjar, D., Taconet, O., Normand, M. and Loumagne, 2000, Land cover discrimination from multitemporal ERS images and multispectral Landsat images: a study case in an agricultural area in France. *International Journal of Remote Sensing*, **21**, pp. 435–456.

Herold, N.D. and Haack, B.N., 2002, Fusion of radar and optical data for land cover mapping. *Geocarto International*, pp. 21–30. Available online at: http://www.informaworld.com/smpp/title~content=t759156373~db=all~tab=issueslist~branches=17 - v1717

Karathanassi, V., Kolokousis, P. and Ioannidou, S., 2007, A comparison study on fusion methods using evaluation indicators. *International Journal of Remote Sensing*, pp. 2309–2341. Available online at: http://www.informaworld.com/smpp/title~content=t713722504~db=all~tab=issueslist~branches=28 - v2828

Li, Z. and Leung, H., 2009, Fusion of multispectral and panchromatic images using a restoration-based method. *IEEE Transactions Geoscience and Remote Sensing*, **5**, pp. 1482–1491.

Mascarenha, N.D.A., Banon, G.J.F. and Candeias, A.L.B., 1996, Multispectral image data fusion under a Bayesian approach. *International Journal of Remote Sensing*, **17**, pp. 1457–1471.

Mather, P.M., 1999, *Computer Processing of Remotely-Sensed Images: An Introduction*, 2nd ed., p. 324 (Chichester: Wiley).

Meher, S.K., Shankar, B.U. and Ghosh, A., 2007, Wavelet-feature-based classifiers for multispectral remote-sensing images. *IEEE Transactions Geoscience and Remote Sensing*, **6**, pp. 1881–1886.

Munechika, C.K., Warnick, J.S., Salvaggio, C. and Schott, J.R., 1993, Resolution enhancement of multispectral image data to improve classification accuracy. *Photogrammetric Engineering and Remote Sensing*, **59**, pp. 67–72.

Pajares, G. and Cruz, J.M., 2004, A wavelet-based image fusion. *Pattern Recognition*, **37**, pp. 1855–1872.

Palubinskas, G. and Datcu, M., 2008, Information fusion approach for the data classification: an example for ERS-1/2 InSAR data. *International Journal of Remote Sensing*, **29**, pp. 4689–4703.

Pohl, C. and van Genderen, J.L., 1998, Multisensor image fusion in remote sensing: concepts, methods and applications. *International Journal of Remote Sensing*, **19**, pp. 823–854.

Ricchetti, E., 2001, Visible-infrared and radar imagery fusion for geological application: a new approach using DEM and sun-illumination model. *International Journal of Remote Sensing*, **22**, pp. 2219–2230.

Richards, J.A. and Jia, S., 1999, *Remote Sensing Digital Image Analysis – An Introduction*, 3rd ed., p. 448 (Berlin: Springer-Verlag).

Saadi, N.M. and Watanabe, K., 2009, Assessing image processing techniques for geological mapping: a case study in Eljufra, Libya. *Geocarto International*, **24**, pp. 241–253.

Saraf, A.K., 1999, IRS-1C-LISS-III and PAN data fusion: an approach to improve remote sensing based mapping techniques. *International Journal of Remote Sensing*, pp. 90–96. Available online at: http://www.informaworld.com/smpp/title~content=t713722504~db=all~tab=issueslist~branches=20 - v2020

Seetha, M., Malleswari, B.L., Muralikrishna, I.V. and Deekshatulu, B.L., 2007, Image fusion – a performance assessment. *Journal of Geomatics*, **1**, pp. 33–39.

Serkan, M., Musaoglu, N., Kirkici, H. and Ormeci, C., 2008, Edge and fine detail preservation in SAR images through speckle reduction with an adaptive mean filter. *International Journal of Remote Sensing*, **29**, pp. 6727–6738.

Serpico, S.B. and Roli, F., 1995, Classification of multisensor remote sensing images by structural neural networks. *IEEE Transactions on Geoscience and Remote Sensing*, **33**, pp. 562–578.

Soh, L.K. and Tsatsoulis, C., 1999, Unsupervised segmentation of ERS and Radarsat sea ice images using multiresolution peak detection and aggregated population equalization. *International Journal of Remote Sensing*, **20**, pp. 3087–3109.

Solberg, A.H.S., Taxt, T. and Jain, A.K., 1996, A Markov random field model for classification of multisource satellite imagery. *IEEE Transactions on Geoscience and Remote Sensing*, **34**, pp. 100–112.

Storvik, G., Fjortoft, R. and Solberg, A.H.S., 2005, A Bayesian approach to classification of multiresolution remote sensing data. *IEEE Transactions Geoscience and Remote Sensing*, **3**, pp. 539–547.

Teggi, S., Cecchi, R. and Serafini, R., 2003, TM and IRS-1C-PAN data fusion using multiresolution decomposition methods based on the 'a trous' algorithm. *International Journal of Remote Sensing*, **24**, pp. 1287–1301.

Teoh, C.C., Mansor, S.B., Mispan, M.R., Mohamed Shariff, A.R. and Ahmad, N. 2001, Extraction of infrastructure details from fused image. In *Proceedings of Geoscience and*

Remote Sensing Symposium, IGARSS' 01. IEEE 2001 International, 3, 9–13 July 2001, Sydney, Australia, pp. 1490–1492.

Verbyla, D.L., 2001, A test of detecting spring leaf flush within the Alaskan boreal forest using ERS-2 and Radarsat SAR data. *International Journal of Remote Sensing*, **22**, pp. 1159–1165.

Vrabel, J., 1996, Multispectral imagery band sharpening study. *Photogrammetric Engineering and Remote Sensing*, **62**, pp. 1075–1083.

Wang, Y., Koopmans, B.N. and Pohl, C., 1995, The 1995 flood in the Netherlands monitored from space – a multisensor approach. *International Journal of Remote Sensing*, **16**, pp. 2735–2739.

Westra, T., Mertens, K.C. and De Wulf, R.R., 2005, ENVISAT ASAR wide swath and SPOT-vegetation image fusion for wetland mapping: evaluation of different wavelet-based methods, *Geocarto International*, **20**, pp. 21–31.

Zhang, J., 2010, Multi-source remote sensing data fusion: status and trends. *International Journal of Image and Data Fusion*, **1**, pp. 5–24.